Photochemical Activity of Nitrogen-Doped Rutile TiO_2(110) in Visible Light

Oliver Diwald,[†] Tracy L. Thompson,[†] Tykhon Zubkov,[†] Ed. G. Goralski,[‡] Scott D. Walck,[‡] and John T. Yates, Jr.*[,†]

Surface Science Center, Department of Chemistry, University of Pittsburgh, Pittsburgh, Pennsylvania 15260, and PPG Industries, Inc., Glass Technology Center, Pittsburgh, Pennsylvania 15238

Received: November 24, 2003; In Final Form: February 23, 2004

TiO_2(110) single crystals, doped with nitrogen via an NH_3 treatment at 870 K, have been found to exhibit photoactivity at photon energies down to 2.4 eV, which is 0.6 eV below the band-gap energy for rutile TiO_2. The active dopant state of the interstitial nitrogen that is responsible for this effect exhibits an N (1s) binding energy of 399.6 eV and is due to a form of nitrogen that is probably bound to hydrogen, which differs from the substitutional nitride state with an N (1s) binding energy of 396.7 eV. Optical absorption measurements also show enhanced absorption down to 2.4 eV for the NH_3-treated TiO_2(110). A co-doping effect between nitrogen and hydrogen is postulated to be responsible for the enhanced photoactivity of nitrogen-doped TiO_2 materials in the range of visible light.

I. Introduction

The photocatalytic and photoelectrochemical applications of semiconducting oxide materials provide a strong scientific incentive for ongoing research.[1−3] Titanium dioxide (TiO_2) belongs to one of the most extensively used and investigated systems and has the advantages of being inexpensive, chemically stable, and nontoxic. Other than the photocatalytic applications of TiO_2, including the degradation of organic pollutants in air and aqueous solutions, it is used for photovoltaic applications[4,5] because it combines good electrical properties with excellent stability in many solvents over a wide pH range. However, because of the rather high intrinsic band gap of rutile TiO_2 (3.0 eV), only 4% of the incoming solar energy on the earth's surface can be utilized. Therefore, considerable efforts have been made to extend the photoresponse of TiO_2-based systems further into the visible-light region, using dopants.

Various transition-metal cation dopants have been extensively investigated.[6−8] However, the disadvantage of cationic dopants is that they can result in localized d-levels deep in the band gap of TiO_2, which often serve as recombination centers for photogenerated charge carriers. Thus, anionic nonmetal dopants, such as carbon,[9] sulfur,[10] and nitrogen,[11] may be more appropriate for extension of photocatalytic activity into the visible-light region, because the related impurity states are supposed to be close to the valence band maximum. Furthermore, the position of the conduction band minimum, which must be kept at the level of the H_2/H_2O potential, when TiO_2 is used for the photoelectrolysis of water into hydrogen and oxygen, is not affected.[12]

With respect to nitrogen-related dopants, Sato reported for the first time that the calcining of mixtures of $Ti(OH)_4$ and ammonium salts leads to TiO_2-based materials that can be activated with visible light.[13] He attributed this beneficial doping effect to NO_x impurities in the TiO_2 lattice. On the basis of a theoretical analysis, Asahi et al.[14] suggested that if nitrogen ions substitute for oxygen in the TiO_2 lattice, the corresponding N (2p) states are located above the valence band edge. By mixing N (2p) states with O (2p) states, the band gap of the nitrogen-doped TiO_2 is reduced and the material should show photoactivity at energies below the intrinsic band gap edge (<3.0 eV). In fact, these authors have proven that films and powders of $TiO_{2-x}N_x$ exhibit a dramatic improvement over pure titanium oxide in their optical absorption below 3.0 eV and of the level of photocatalytic activity for visible light. Irie et al.[15] measured higher quantum yields for the decomposition of gaseous 2-propanol on $TiO_{2-x}N_x$ with UV light than with visible light and concluded that the nitrogen-induced effect allowing sub-band-gap excitation is due to an isolated N (2p) state rather than to narrowing of the band gap. Lindgren et al.[16] used photoelectrochemical measurements to confirm that the nitrogen-created states are located close to the valence band maximum and that the conduction band edge remains unchanged by nitrogen doping.

Generally, polycrystalline nitrogen-doped samples have been produced by different preparative procedures: (i) reactive sputtering of TiO_2 targets with nitrogen/argon gas mixtures for films, and (ii) hydrolysis of NH_x/TiO_2 mixtures or thermal treatment of TiO_2 in a NH_3 atmosphere for powder samples. In a recent single-crystal study, we have shown that ion implantation of atomically clean TiO_2(110) surfaces with mixtures of N_2^+ and Ar^+ ions, followed by subsequent annealing under ultrahigh-vacuum conditions, is an effective way to incorporate nitrogen into the TiO_2 lattice.[17] X-ray photoelectron spectroscopy (XPS) revealed exclusively a N (1s) feature at a binding energy of 396.6 eV that is attributed to substitutionally bound nitride nitrogen.[11] In contrast to expectations, these nitrogen-doped crystals, which contained only nitride ions, exhibited a shift in the photothreshold energy of 0.2 eV to *higher* energy, compared to undoped TiO_2(110), as measured by the photodesorption of molecular oxygen.[16]

In the present study, we have used another method to dope TiO_2(110) with nitrogen, and we have found that the photothreshold energy can be shifted 0.6 eV in a *desirable* direction to *lower* energy. The new method of nitrogen doping involves

* Author to whom correspondence should be addressed. E-mail address: jyates@pitt.edu.
[†] University of Pittsburgh.
[‡] PPG Industries.

10.1021/jp031267y CCC: $27.50
Published on Web 04/17/2004

high-temperature treatment of TiO_2(110) with NH_3 gas and is observed to produce an additional subsurface N (1s) feature at 399.6 eV.

To determine the photoactivity in the threshold region of rutile (<3 eV), the photochemical reduction of Ag^+ ions in aqueous solutions was measured.[18−20] The capture of photogenerated electrons on the TiO_2 surface by Ag^+ ions causes the deposition of metallic silver and can, therefore, be directly used for quantification of the photoeffect on TiO_2. This was done for the first time by Fleischauer et al.,[18] who measured reaction rates and quantum efficiencies on ZnO and TiO_2 single-crystal surfaces by monitoring changes in the optical reflectivity due to the formation of metallic silver. By means of atomic force microscopy (AFM), Farneth and co-workers used the photocatalytic reduction of Ag^+ ions on polycrystalline TiO_2 films to investigate changes in the photoactivity of different rutile crystal faces.[19,20] This method has been extended to assess the photoactivity of individual TiO_2 particles.[21]

II. Experimental Section

Polished TiO_2(110) single-crystal substrates (Princeton Scientific Corporation, Princeton, NJ) were treated in a flow reactor system in an argon gas atmosphere (1 atm) at 870 K. Typical heating rates were 7 K/min. For doping, the argon flow was replaced by NH_3 for 5 min, after the target temperature had been reached. Subsequently, the crystals were kept in flowing argon for 1 h at 870 K and then cooled in flowing argon over a time period of 2−3 h. Optical absorption spectra were acquired with a Perkin−Elmer Lambda 9 spectrophotometer.

For the silver reduction assay, doped and undoped crystal substrates were cleaved into slices ~1 mm × 5 mm in size and then mounted pairwise on an optical microscope slide. Six to ten slices of the NH_3-treated and the blank crystal were assembled in two columns and immersed in an aqueous 0.1 N $AgNO_3$ solution, which covered the sample surface to a depth of 3 mm. Illumination was performed with a 500-W high-pressure mercury lamp (Oriel). For light exposure of selected energy, the light beam was first passed through a water filter, to eliminate effects from IR radiation. Interference filters of selected wavelength, with a bandwidth of 10 nm (Andover Corporation), were used. The radiation intensity was measured at the sample position over the spectral region of interest, using a thermopile detector (Oriel model 71751) as a primary standard. The incident UV light intensity at the position of the sample surface, depending on the photon energy, was in the range of 1−4 mW/cm^2. Typical light exposure times were 1−5 min, which corresponded to photon fluxes of the order of 10^{17} photons/cm^2.

After sample exposure to light of defined energy and photon flux, the mounted crystals were rinsed, first in distilled water and then in ethanol. Remaining liquids were removed from the sample surface by blowing with dry air and subsequent drying in an oven for 40 min at 140 °C in air.

Imaging of the silver deposits on the TiO_2 surface was performed using AFM (Nanoscope IIIa Dimension 3100, from Digital Instruments). The probe tips used in this investigation were silicon nitride and were obtained from Veeco (model DNP-20). Images were collected in contact mode and were used to directly obtain information relating to the height and overall shape of the deposited silver clusters. Typical lateral scan frequencies were 1.5 Hz.

For quantification of the deposited silver, a flooding algorithm of the WSxM 4.0 software package (Nanotec Electronica S.L.) was used. The volume covered by silver clusters, per square centimeter, was taken as a measure of the quantity of deposited silver. Tip convolution effects, as well as the volume contribution from the detected silver clusters below a threshold of 2 nm, were neglected in this evaluation, and errors due to these two simplifications have a tendency to cancel each other. Values for the quantum yield were calculated as the number of Ag atoms produced per square centimeter, divided by the total number of photons per square centimeter impinging on the surface.

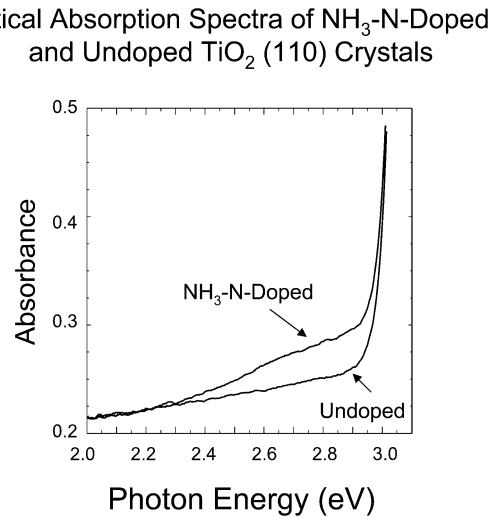

Figure 1. Absorption spectra of nitrogen-doped and undoped rutile TiO_2 single crystals measured at room temperature. The data have not been corrected for reflection loss.

XPS measurements were performed at the PPG Glass Technology Center. The XPS spectra were acquired with a spectrometer (Vacuum Generators, model ESCALAB Mk II), using unmonochromatized Mg Kα X-rays (240 W). Measurements via XPS and Ar^+ sputtering steps (4 keV, $I = 4\ \mu$A/cm^2) were performed in a high-vacuum chamber with a base pressure of 10^{-8} Torr. The binding energy of the N (1s) peaks were calibrated with respect to the O (1s) peak from TiO_2 at 530.2 eV. The nitrogen concentration was estimated from the relative area intensities of the N (1s), Ti (2p), and O (1s) peaks. They were normalized using relative sensitivity factors in the Vacuum Generators software package.

III. Results and Discussion

A. Photoabsorption Spectrum. The absorption spectrum in Figure 1 reveals the fundamental absorption edge of rutile at 3.0 eV on both a nitrogen-doped rutile and an undoped rutile TiO_2(110) single crystal. However, the nitrogen-doped crystal, which was produced via thermal treatment in an ammonia atmosphere, also has an increased optical absorption in the range of 2.4−3.0 eV. These crystals, after they have been doped, are bluish-green in color, whereas the undoped crystals are slightly yellowish in color, yet clear. The color of the nitrogen-doped crystals is partially due to the bulk reduction of the crystal, because the thermal decomposition of NH_3 on the TiO_2 surface results in the evolution of molecular hydrogen, which reduces the crystal electronically.[22,23] In addition, the presence of the absorption band below the edge at 3 eV indicates that nitrogen penetrates into the single crystal and effectively changes the electronic structure of the solid.

B. Silver Deposition on the Surface of Doped and Undoped TiO_2 Crystals. For investigation of the photocatalytic activity in the near-threshold region (2.3 eV ≤ $h\nu$ ≤ 3.0 eV), the silver deposition method was applied, using defined numbers of

TABLE 1: Energy Dependence of Silver Deposition on Undoped and Nitrogen-Doped Rutile TiO_2 Single Crystals

		Undoped TiO_2 Crystal			Nitrogen-Doped TiO_2 Crystal		
energy (eV)	number of photons ($\times 10^{17}$ cm^{-2})	number of images	silver concentration ($\times 10^{-9}$ mol/cm^2)	standard deviation	number of images	silver concentration ($\times 10^{-9}$ mol/cm^2)	standard deviation
dark	0	8	0.2	0.3	6	0.6	0.7
3.16	4.2	12	241.4	81.8	12	136.3	124.6
2.98	5.6	12	5.6	4.5	11	21.7	4.6
2.85	6.5	18	4.3	2.0	10	14.7	7.3
2.70	2.3	10	1.1	0.7	8	3.6	1.5
2.47	8.6	10	0.3	0.2	10	1.6	0.8
2.27	8.2	6	0.3	0.3	10	0.3	1.1

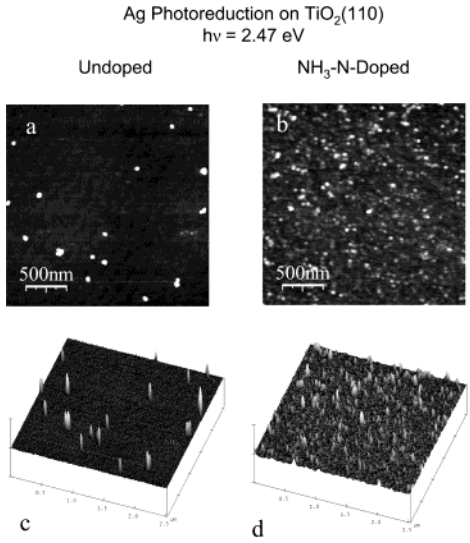

Figure 2. Contact-mode AFM images of silver deposits on the surface of (a and c) undoped and (b and d) NH_3-nitrogen-doped TiO_2 single crystals after photoreduction with $h\nu = 2.47$ eV. Black-to-white vertical contrast in panels a and b (two-dimensional (2D) images) is 5 nm, whereas the three-dimensional (3D) representations in panels c and d have a vertical scale of 20 nm.

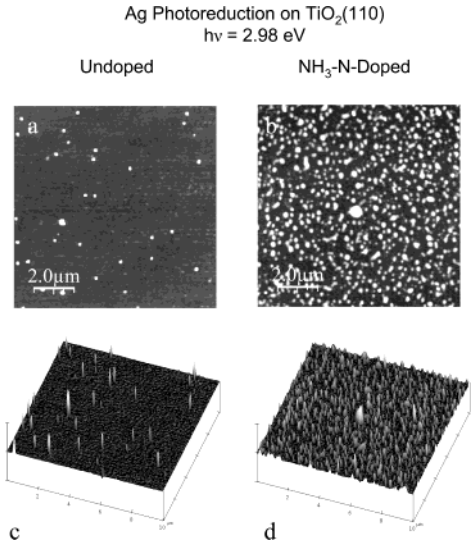

Figure 3. Contact-mode AFM images of silver deposits on the surface of (a and c) undoped and (b and d) NH_3-nitrogen-doped TiO_2 single crystals after photoreduction with $h\nu = 2.98$ eV. Black-to-white vertical contrast in panels a and b (2D images) is 10 nm, whereas the 3D representations in panels c and d have a vertical scale of 50 nm.

photons passing through 10-nm windows in the optical filters. Although unilluminated crystal surfaces exhibit only small noticeable changes before and after contact with the $AgNO_3$ solution (for quantification, see Table 1), the deposition of silver clusters on the doped crystal surfaces was significant after exposure to visible light below $h\nu = 3.0$ eV. Figures 2a and b show typical topographic AFM images that have been obtained on samples after light excitation with $h\nu = 2.47$ eV. The contrast results from vertical height differences on the surface, where black is low and white is high. Three-dimensional (3D) topographic reconstructions from the same data sets are displayed in Figures 2c and d. The doped and irradiated surface clearly is homogeneously covered by silver clusters with heights of 3−10 nm, whereas the surface of the undoped crystal contains only a limited number of clusters, which are inhomogeneously distributed. When the same experiment was performed with $h\nu = 2.98$ eV (Figures 3a and b), the silver deposition rate was dramatically enhanced and silver clusters with average heights of 10 nm are imaged via AFM. For quantification of the silver concentration, the average volume of these silver clusters, per square centimeter, was derived from the AFM data. Based on 6−18 scans of different regions of every sample surface, the average concentration is shown in Table 1 as a function of photon energy. Assuming that each Ag atom originates from a photogenerated electron, the quantum yield[22] was calculated for the near-threshold region (<3.0 eV) and plotted as a function of photon energy, as shown in Figure 4.[24] In the near-threshold region (<3.0 eV), the concentration of deposited silver on the nitrogen-doped crystal was greater than that for the undoped

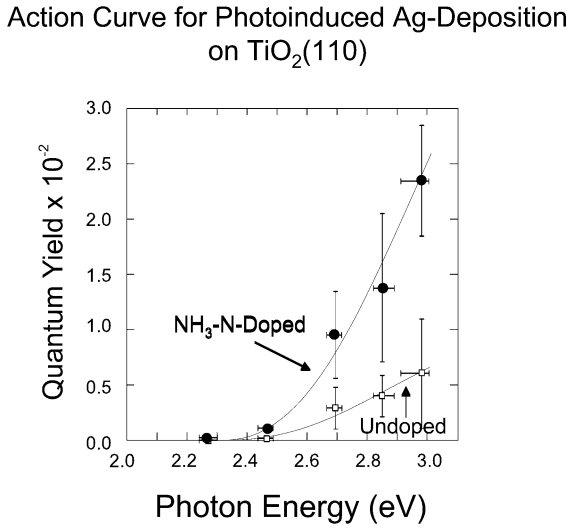

Figure 4. Action curve, showing the quantum yield versus excitation energy for the photoreduction of silver on the surface of undoped and NH_3-nitrogen-doped TiO_2 single crystals. Error bars in the quantum yield are based on the standard deviation from measurements on 8−18 images from different regions of the crystal (see Table 1). Error bars in photon energy correspond to the bandwidth of the interference filters used, where the location of the point is the band maximum of the respective filter transmission spectrum.

crystal (by a factor of 2 ($h\nu = 2.47$ eV) to 4 ($h\nu = 2.98$ eV)), which proves the substantial photocatalytic activity of the NH_3-treated crystal in the visible-light spectral range. The threshold

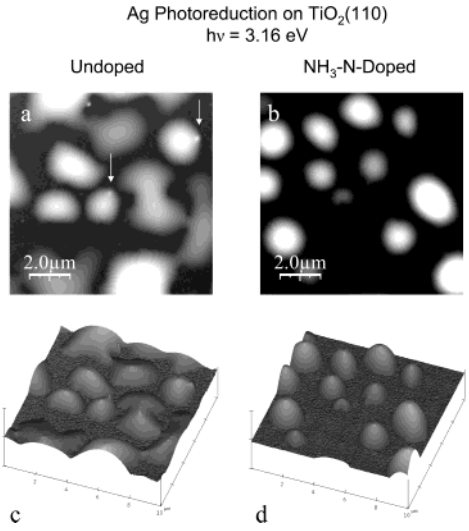

Figure 5. Contact-mode AFM images of silver deposits on the surface of (a and c) undoped and (b and d) NH_3-nitrogen-doped TiO_2 single crystals after photoreduction with $h\nu = 3.16$ eV. Black-to-white vertical contrast in panels a and b (2D images) is 100 nm, whereas the 3D representations in panels c and d have a vertical scale of 200 nm.

photon energy for silver deposition on the nitrogen-doped TiO_2-(110)—which is ~2.4 eV—is in good agreement with the optical absorption spectrum in Figure 1.

Higher rates for silver deposition were observed after irradiation experiments with a supra-band-gap photon energy (e.g., $h\nu = 3.16$ eV; see Figures 5a and c), leading to a much more complex topography of silver deposits. Different from all sub-band-gap experiments, both doped and undoped TiO_2 surfaces produce large silver islands with heights of 50−170 nm. The existence of much-smaller clusters, as indicated by arrows in Figure 5, suggests that the large features emerge from the coalescence of many primary particles during photodeposition or during the drying procedure at 310 K. The average silver concentration was determined to be $(2.41 \pm 0.8) \times 10^{-7}$ mol/cm^2 for an undoped crystal and (1.36 ± 1.25) 10^{-7} mol/cm^2 for the nitrogen-doped crystal. The large values for the standard deviations reflect the fact that, on both sample surfaces, some areas are uniformly coated, whereas others exhibit an inhomogeneous distribution of elevated features. The quantum yields at $h\nu = 3.16$ eV for the undoped and the doped samples are 0.35 and 0.2, respectively. These values are too high, considering that the (110) orientation of rutile TiO_2 is an order of magnitude less photochemically reactive than the (101) plane, for which quantum yields between 0.6 and 0.4 were reported.[19,20] Together with the inhomogeneous distribution of silver, this suggests the presence of autocatalytic reactions during silver reduction with light that has supra-band-gap energy.

C. X-ray Photoelectron Spectroscopy. For chemical identification of the valence state of the dopant nitrogen, XPS was used. Surface analysis on doped and undoped TiO_2(110) showed an impurity XPS feature that was centered at 399.6 eV. UV treatment in air and/or removal of the first 5 Å of the surface by sputtering with Ar^+ ions lead to the extensive depletion of these signals (Figure 6a). These traces of nitrogen must be attributed to surface contamination, which probably originates from spurious NH_3 in the flow reactor chamber. Their presence only on the surface excludes their role in the enhanced optical activity in the range of visible light. However, after the removal of 60 Å of TiO_2 by Ar^+ sputtering, two N (1s) features at 399.6 and 396.7 eV are observed, which indicates the presence of bulk nitrogen in two different chemical states. The total nitrogen

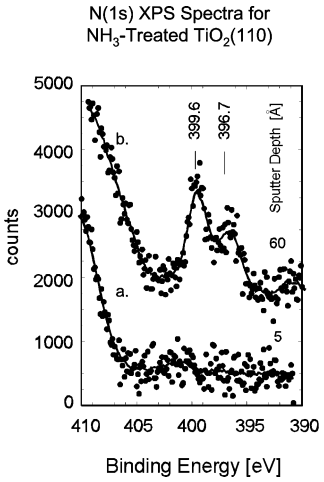

Figure 6. Nitrogen (N 1s) spectrum from a doped TiO_2(110) crystal at two different Ar^+ sputter depths: (a) 5 Å and (b) 60 Å.

concentration at 60 Å was determined to be ~0.6 at. %. The feature at 396.7 eV is generally known as the "nitride" peak and has been assigned to N^{2-} anions, which substitute for oxygen in the TiO_2 lattice.[25] As indicated by the smaller chemical shift, the nitrogen species that is associated with the feature at 399.6 eV carries less negative charge than a nitride ion. The value for the binding energy agrees well with XPS data from NH_x-containing compounds[26] and suggests that the 399.6 eV N (1s) species is chemically bound to hydrogen.

Our previous studies of nitrogen implantation into TiO_2(110) have shown that the photochemical absorption edge is shifted 0.2 eV to *higher* energy and that the substitutional nitride ion with an N (1s) binding energy of 396.7 eV is the only subsurface dopant species present.[17] This nitride species is probably also produced by the Ar^+ ion sputtering method used to expose the subsurface region for XPS analysis in these experiments. This causes partial conversion into the nitride of nitrogen introduced by NH_3 doping at 870 K. We thus assign the nitrogen state (N (1s) = 399.6 eV) introduced by NH_3 as being responsible for the shift of the photochemical threshold, down to ~2.4 eV. This form of nitrogen is most likely located in an interstitial site, and this form of nitrogen dopant is probably bound to hydrogen. These results disagree with the conclusions of Asahi et al.,[14] who reported that nitride ions that substitute for O^{2-} ions in the TiO_2 lattice are the necessary dopant species for TiO_2 photocatalysis in the visible-light region.

D. Comparison of Nitrogen-Doping Effects in TiO_2 with Those in ZnO. Although the effect of nitrogen doping in TiO_2-(110) is clearly shown in this work, the explanation for this effect is still somewhat under debate. The effect of doping in other wide-band-gap semiconductors, such as zinc oxide, for example, has recently also been studied. Zinc oxide (ZnO) is another *n*-type semiconductor, similar to TiO_2, with an intrinsic band gap of $E_g = 3.3$ eV. In ZnO, nitrogen as a dopant should produce shallow acceptor levels within the band gap. However, at this point in time, no one has successfully obtained *p*-type ZnO using a pure nitrogen source.[27] On the other hand, the co-doping of nitrogen, in conjunction with hydrogen or gallium, has been shown to be successful.[28,29] The presence of donor dopants, as suggested by Yamamoto,[30] has two consequences that may also apply to N:H-doped TiO_2. The first is an enhanced incorporation of acceptors, because of their strong electrostatic attractive interaction, which leads to higher acceptor (nitrogen) incorporation in TiO_2. The second consequence is the lowering of the acceptor energy level, bringing the level closer to the

valence band. A hybridized state (N p-orbitals and H s-orbitals) is postulated to be formed in TiO_2, by analogy to ZnO. Both effects are beneficial for the enhanced optical absorption of ZnO[28] and might also explain the photoactivity of N:H-doped TiO_2 in the visible spectral range.

IV. Conclusion

These findings, in conjunction with a recent investigation of nitrogen-implanted $TiO_2(110)$,[16] indicate that nitrogen with an N (1s) binding energy of 399.6 eV is effective in reducing the threshold photon energy for photochemistry from 3.0 eV to 2.4 eV, which is a shift of 0.6 eV into the visible spectral region. This form of nitrogen can be introduced into the TiO_2 bulk via heat treatment in NH_3 at 870 K. This active nitrogen is likely to be interstitial and chemically bound to hydrogen in the first few hundred Ångstroms below the TiO_2 surface. In contrast, substitutional nitrogen, in the form of implanted nitride species, is inactive for lowering the photochemical threshold energy below the band-gap energy of rutile TiO_2 ($E_g = 3.0$ eV). These findings are in contrast to current scientific opinion.

Acknowledgment. This work was supported by the DoD Multidisciplinary University Research Initiative (MURI) program, administered by the Army Research Office, under Grant No. DAAD-19-01-0-0619. We would like to thank Yujie Sun for helpful advice and direction with the AFM measurements made at the University of Pittsburgh. Special thanks to Pittsburgh Plate Glass (PPG) for scientific collaboration and analytical services.

References and Notes

(1) Linsebigler, A.; Lu, G.; Yates, J. T., Jr. *Chem. Rev.* **1995**, *95*, 735−758.
(2) Hoffmann, M. R.; Martin, S. T.; Choi, W.; Bahnemann, D. W. *Chem. Rev.* **1995**, *95*, 69−96.
(3) Serpone, N., Pilezzetti, E. Eds. *Photocatalysis: Fundamentals and Applications*; Wiley-Interscience: New York, 1989.
(4) Fujishima, A.; Honda, K. *Nature* **1972**, *238*, 37−38.
(5) O'Regan, B.; Gratzel, M. *Nature* **1991**, *353*, 737−739.
(6) Choi, W.; Termin, A.; Hoffmann, M. R. *J. Phys. Chem. B* **1994**, *94*, 13669−13679.
(7) Hermann, J. M.; Disdier, J.; Pichat, P. *Chem. Phys. Lett.* **1984**, *108*, 618−622.
(8) Anpo, M.; Takeuchi, M. *J. Catal.* **2003**, *216*, 505−516.
(9) Khan, S. U. M.; Al-Shahry, M.; Ingler, W. B., Jr. *Science* **2002**, *297*, 2243−2245.
(10) Umebayashi, T.; Yamaki, T.; Itoh, H.; Asai, K. *Appl. Phys. Lett.* **2002**, *81*, 454−456.
(11) Morikawa, T.; Asahi, R.; Ohwaki, T.; Aoki, K.; Taga, Y. *Jpn. J. Appl. Phys.* **2001**, *40*, L561−L563.
(12) Hagfeldt, A.; Grätzel, M. *Chem. Rev.* **1995**, *95*, 49−68.
(13) Sato, C. S. *Chem. Phys. Lett.* **1986**, *123*, 126−128.
(14) Asahi, R.; Morikawa, T.; Ohwaki, T.; Aoki, K.; Taga, Y. *Science* **2001**, *293*, 269−271.
(15) Irie, H.; Watanabe, Y.; Hashimoto, K. *J. Phys. Chem. B* **2003**, *107*, 5483−5486.
(16) Lindgren, T.; Mwabora, J. M.; Avendaño, E.; Jonsson, J.; Hoel, A.; Granqvist, C.-G.; Lindquist, S.-E. *J. Phys. Chem. B* **2003**, *107*, 5709−5716.
(17) Diwald, O.; Thompson, T. L.; Goralski, E. G.; Walck, S. D.; Yates, J. T., Jr. *J. Phys. Chem. B* **2004**, *108*, 52−57.
(18) Fleischauer, P. D.; Kann, H. K. A.; Shepherd, J. R. *J. Am. Chem. Soc.* **1972**, *94*, 283−285.
(19) Hotsenpiller, P. A. M.; Bolt, J. D.; Farneth, W. E.; Lowekamp, J. B.; Rohrer, G. S. *J. Phys. Chem. B* **1998**, *102*, 3216−3226.
(20) Lowenkamp, J. B.; Rohrer, G. S.; Hotsenpiller, P. A.; Bolt, J. D.; Farneth, W. E. *J. Phys. Chem. B* **1998**, *102*, 7323−7327.
(21) Farneth, W. E.; McLean, R. S.; Bolt, J. D.; Dokou, E.; Barteau, M. A. *Langmuir* **1999**, *15*, 8569−8573.
(22) Rekoske, J. E.; Barteau, M. A. *J. Phys. Chem. B* **1997**, *101*, 1113−1124.
(23) This produces a broad optical absorption (from 0.5 eV to 2 eV) that is associated with electronically reduced defects in the bulk (not shown in Figure 1).
(24) The accuracy of the quantum yield in Table 1 is dependent on the validity of the assumptions made, i.e., neglect of tip convolution effects and neglect of features below the 2-nm threshold. The AFM probe has a finite radius; therefore, the lateral dimensions of small protruding features from the surface are systematically overestimated. Thus, the values in Table 1 are an upper limit for the actual quantum yields.
(25) Saha, N. C.; Tompkins, H. G. *J. Appl. Phys.* **1992**, *72*, 3072−3079.
(26) Souto, S.; Alvarez, F. *Appl. Phys. Lett*. **1997**, *70*, 1539−1541 and references therein.
(27) Lee, E.-C.; Kim, Y.-S.; Jin, Y.-G.; Chang, K. J. *Phys. Rev. B* **2001**, *64*, 085120 (1−5).
(28) Minegishi, K.; Koiwai, Y.; Kikuchi, Y.; Yano, K.; Kasuga, M.; Shimizu, A. *Jpn. J. Appl. Phys.* **1997**, *36*, L1453−L1455.
(29) Joseph, M.; Tabata, H.; Kawai, T. *Jpn. J. Appl. Phys.* **1999**, *38*, L1205−L1207.
(30) Yamamoto, T. *Thin Solid Films* **2002**, *421*, 100−106.